Physics Letters A ••• (••••) •••–•••

Contents lists available at ScienceDirect

Physics Letters A

www.elsevier.com/locate/pla

Solitons in $\mathcal{PT}$-symmetric SRR dimers chain with alternating electric and magnetic coupling

Wei-na Cui [a], Hong-xia Li [a], Min Sun [a], Ling-bing Bu [b]

[a] Department of Applied Physics, Nanjing University of Science and Technology, Nanjing 210094, PR China
[b] Collaborative Innovation Center on Forecast and Evaluation of Meteorological Disasters, Key Laboratory for Aerosol-Cloud-Precipitation of China Meteorological Administration, Key Laboratory of Meteorological Disaster of Ministry of Education, Nanjing University of Information Science and Technology, Nanjing 210044, PR China

ARTICLE INFO

Article history:
Received 26 June 2017
Received in revised form 11 September 2017
Accepted 12 September 2017
Available online xxxx
Communicated by C.R. Doering

Keywords:
$\mathcal{PT}$-symmetry
Split-ring resonator
Nonlinear
Solitons

ABSTRACT

Dynamics of a $\mathcal{PT}$-symmetry chain comprising split-ring resonator (SRR) dimers with both gain and loss are investigated. A dimer is built as a pair of opposite orientations of the SRR gaps which result in the alternating electric and magnetic coupling in the chain. The transition from the exact to the broken $\mathcal{PT}$-symmetric phase is presented in the linear regime. Considering the Kerr nonlinearity, it is shown that the localized modes in the form of solitons exist in the continuum limit approximation. Such localized structures are studied in the phase plane and numerical expressions are also obtained.

© 2017 Elsevier B.V. All rights reserved.

UNCORRECTED PROOF

1. Introduction

The topic of parity-time ($\mathcal{PT}$)-symmetry have drawn considerable attention from both the physics and the mathematics communities [1–4]. The $\mathcal{PT}$-symmetry theme started out from non-Hermitian quantum mechanics, where a complex but $\mathcal{PT}$-symmetric potential could possess all-real spectrum [5,6]. This concept has been recently extended to dynamical lattices, particularly in optics, where photonic lattices are arranged by gain and loss elements [3,7,8]. It is shown that $\mathcal{PT}$-symmetric systems can possess a spontaneous symmetry-breaking phase transition with an eigen energy transition from real spectra into complex spectra, creating physical properties of quantum mechanics in classical systems. Moreover, nonlinear effect in $\mathcal{PT}$-symmetric systems is a natural extension of applications. The formation of localized modes, nonlinearly-induced $\mathcal{PT}$-symmetric breaking, stable Talbot effects,and all-optical switching was theoretically demonstrated [9–13].

Split ring resonator (SRR) is an important building block of metamaterials which exhibits electromagnetic properties not found in nature [14]. The near-field patterns of metamaterial elements has a crucial interplay between the magnetic coupling and electric coupling. This means that the way of the arrangement of resonators in a lattice or superlattice plays an important role in determining the response of the metamaterial [15–18]. Magnetoinductive waves were proved to exist on SRRs arrays due to magnetic and electric coupling between individual magnetic meta-atoms [19–22]. Embedding meta-atoms into nonlinear host media provides strong nonlinear response particularly for THz, infrared, and optical resonant elements [23]. Due to the combination of nonlinearity and discreteness in metamaterials arrays, certain types of nonlinear excitations may exist predicted in Ref. [24,25]. Recently, the reference [26] introduced a particular $\mathcal{PT}$-symmetric nonlinear system constructed by SRR dimers having both gain and loss. The nonlinear localized modes are exist as a result of the gain and dissipation matching. In paper [13] the authors presented the modulation theory in $\mathcal{PT}$-symmetric magnetic metamaterial arrays in the continuum limit which the gap soliton solutions and symmetry breaking phenomenon at a critical value of the gain or loss term were obtained. However, in the above $\mathcal{PT}$-symmetric nonlinear dimer SRRs chain the magnetic interaction is dominant, but the electric interaction is neglected. We will present a different configuration of the dimer SRRs chain in this paper, not only the magnetic

E-mail address: cuiweinaa@163.com (W.-n. Cui).

https://doi.org/10.1016/j.physleta.2017.09.021
0375-9601/© 2017 Elsevier B.V. All rights reserved.

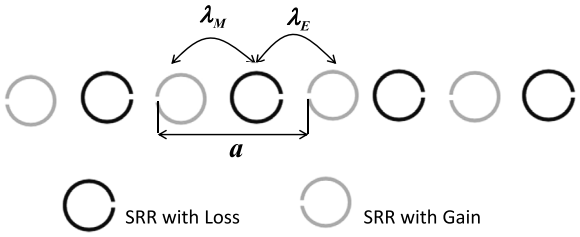

Fig. 1. Schematic of the chain of SRR dimers with alternating magnetic coupling λ_M and electric coupling λ_E.

coupling is considered but also the electric coupling. In the following we will study the nonlinear excitations in a $\mathcal{PT}$-symmetric dimer SRRs chain with alternating electric and magnetic coupling. First, the model is introduced which involves a set of difference-differential equations and the $\mathcal{PT}$-symmetric phase of this system is presented. Secondly, the asymptotic expansions are provided and the amplitude equations in the continuum approximation are derived. The nonlinear excitations in the form of localized modes are studied in the phase plane and numerical expressions are also obtained. Finally, we contain a discussion and summary of our results.

2. Physical model

A metadimer comprises two SRRs with the same size, but with the opposite orientations of the SRR gaps shown in Fig. 1. If the gaps in neighboring elements are next to each other, the SRRs are coupled through the electric dipoles developed in their gaps, and the dominant coupling is electrical. But in another case, the gaps are on opposite sides, the magnetic field induces an electromotive force which in turn produce currents coupled the neighboring SRRs, and the dominant coupling is magnetic through their mutual inductance [15]. As a result, each individual SRR couples to its neighboring SRRs due to both magnetic and electric interaction. We take the metadimer as the unit to form a diatomic chain with the period a. Some linear properties without loss has been studied in Ref. [21]. In order to satisfy the requirements for $\mathcal{PT}$-symmetry, we assume one SRR of the metadimer has gain while the other has equal amount of loss. Using the coupled LC-resonator scheme each individual SRR can be taken as an LC circuit with self-inductance L, Ohmic resistance R, and capacitance C. If one fills the gap of each SRRs Kerr dielectric the units provide their nonlinear properties as shown in Ref. [23–25]. In the equivalent circuit model picture [21,24,26], extended for the $\mathcal{PT}$-symmetry dimer chain with alternating electric and magnetic coupling, the equations describing the dynamics of the charge $Q_n(q_n)$ in nth SRR can be described by

$$\frac{d^2}{dt^2}(Q_n+\lambda_M q_{n+1})+\lambda_E q_n+Q_n-\frac{\alpha}{3\epsilon_l}Q_n^3+\gamma\frac{dQ_n}{dt}=0, \tag{1}$$

$$\frac{d^2}{dt^2}(q_n+\lambda_M Q_{n+1})+\lambda_E Q_n+q_n-\frac{\alpha}{3\epsilon_l}q_n^3-\gamma\frac{dq_n}{dt}=0, \tag{2}$$

where λ_M and λ_E are the magnetic and electric interaction coefficients respectively, and γ is the gain or loss coefficient ($\gamma>0$). In our the planar configuration shown in Fig. 1, we note the magnetic coupling is negative $\lambda_M<0$, whereas the electric coupling is positive $\lambda_E>0$. The parameter ϵ_l represents the linear permittivity and $\alpha=+1(-1)$ accounts for self-focusing (defocusing) nonlinearity of the Kerr-type medium embedded in each SRRs. The electromotive forcing is not considered in our model. There exists the guided electromagnetic waves called magnetoinductive waves due to the alternating magnetic and electric coupling between the elements in the chain of SRRs. By substituting magnetoinductive plane wave solutions $Q_n=C\exp[i(kn-\omega t)]$ and $q_n=D\exp[i(kn-\omega t)]$ into Eqs. (1) and (2), where ω and k are angular frequency and normalized wavenumber respectively, C and D are amplitudes, and Eqs. (1) and (2) lead to the following equations in the linear case

$$(-\omega^2\lambda_M e^{ik}+\lambda_E e^{-ik})C+(-\omega^2+1-i\omega\gamma)D=0, \tag{3}$$

$$(-\omega^2+1+i\omega\gamma)C+(-\omega^2\lambda_M e^{-ik}+\lambda_E e^{ik})D=0. \tag{4}$$

The condition of the vanishing of the determinant of this linear system leads to a quadratic equation for ω^2 with solutions

$$\omega_{\pm}^2=\frac{(2+2\lambda_M\lambda_E\cos k-\gamma^2)\pm\{(2+2\lambda_M\lambda_E\cos k-\gamma^2)^2-4(1-\lambda_M^2)(1-\lambda_E^2)\}^{1/2}}{2(1-\lambda_M^2)}. \tag{5}$$

The stable phase (unbroken $\mathcal{PT}$-symmetry) corresponds to the case where ω is a real quantity. From straightforward examination of Eq. (5), one concludes that the condition for ω being real for any k is $\gamma\le\gamma_c$ with $\gamma_c=\{2+2\lambda_M\lambda_E-2[(1-\lambda_M^2)(1-\lambda_E^2)]^{1/2}\}^{1/2}$. In this exact phase ($\gamma\le\gamma_c$), the $\mathcal{PT}$-symmetry dimer chain has two branches and exhibits a gap at the Brillouin-zone edge $k=0$. We note the eigenvalues are determined by the magnetic and electric coupling as well as the gain/loss coefficient γ. With the gain/loss coefficient γ increased, the gap width of two branches decreases, and the gap closes at $\gamma=\gamma_c$, seen in Fig. 2. A phase diagram on the $\gamma-\lambda$ plane, with $\lambda=\lambda_M/\lambda_E$, is shown in Fig. 3. For fixed λ_M, the bandwidths is a function of γ and λ. The stability window in $\gamma-\lambda$ space is given by the area under the curve γ_c. For $\gamma>\gamma_c$, some frequencies in the spectrum acquire imaginary parts and $\mathcal{PT}$-symmetry breaking occurs. Fig. 3 exhibits the stability region and also the square frequencies as a function of the gain/loss parameter γ. Furthermore, if the magnetic coupling and electric coupling have the same value $|\lambda_M|=\lambda_E$, the frequency ω shown in Eq. (5) has always imaginary parts for all k for any $\gamma>0$, and the system will always be in the broken $\mathcal{PT}$-symmetric phase.

UNCORRECTED PROOF

Please cite this article in press as: W.-n. Cui et al., Solitons in $\mathcal{PT}$-symmetric SRR dimers chain with alternating electric and magnetic coupling, Phys. Lett. A (2017), https://doi.org/10.1016/j.physleta.2017.09.021

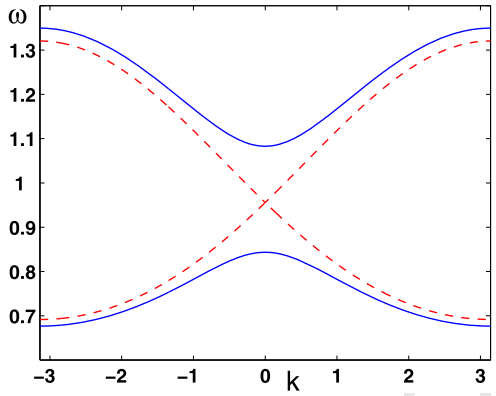

Fig. 2. Dispersion diagrams for the chain of SRR dimers with $\lambda_M = -0.21$, $\lambda_E = 0.45$. Solid and dash lines correspond to the $\gamma = 0.1$ and $\gamma = \gamma_c = 0.25$ respectively.

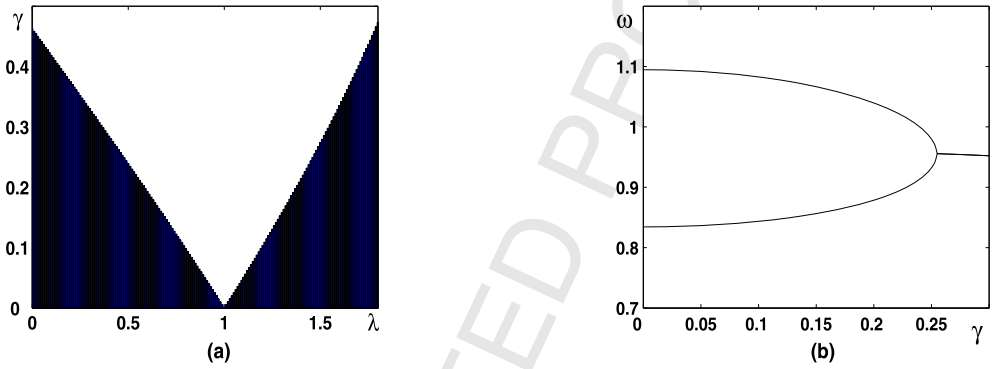

Fig. 3. (a) There is the exact phase region (shaded) under the curve $\gamma = \gamma_c(\lambda)$ with $\lambda = \lambda_M/\lambda_E$, and the system is unstable corresponding to the broken phase outside $\gamma = \gamma_c(\lambda)$ for $\lambda_E = 0.45$. (b) Frequency band boundaries as a function of the gain and loss parameter γ for $\lambda_M = -0.21$, $\lambda_E = 0.45$.

3. Solitons solutions

Because in general it is not possible to solve analytically nonlinear lattice equations such as Eqs. (1) and (2), some approximate theories have been developed. One powerful and clear-cut method is the method of quasidiscreteness approach, widely used in the study of nonlinear waves, solitons, and pattern formation in discrete system. The basic spirit of the quasidiscreteness approach is the assumption that a linear plane lattice wave is weakly modulated by the nonlinearity of the system [13,24,25]. Here we use the continuum approximation given by the expansions as following to analyze the long-wave limit case

$$Q_{n+1}(t) = W(x,t) + W_x(x,t) + \frac{1}{2}W_{xx}(x,t) + ..., \tag{6}$$

$$q_{n-1}(t) = V(x,t) - V_x(x,t) + \frac{1}{2}V_{xx}(x,t) + ..., \tag{7}$$

with $x = na$, when returning to the original variables. For the first-order approximation we obtain

$$W_{tt} + W + \lambda_M V_{tt} - \lambda_M V_{ttx} - \lambda_E V + \gamma W_t - \frac{\alpha}{3\epsilon_l}W^3 = 0, \tag{8}$$

$$V_{tt} + V + \lambda_M W_{tt} + \lambda_M W_{ttx} - \lambda_E W - \gamma V_t - \frac{\alpha}{3\epsilon_l}V^3 = 0. \tag{9}$$

Assuming the parameters $\lambda_E, \lambda_M, \gamma$ are small, we describe in some detail the weakly nonlinear theory for the continuum model. Let

$$W = W_0 + \varepsilon W_1 + \varepsilon^2 W_2 + ... \quad V = V_0 + \varepsilon V_1 + \varepsilon^2 V_2 + ..., \tag{10}$$

where $0 < \varepsilon \ll 1$ is a small parameter. To the leading order the linear equations are obtained as

$$W_{0tt} + V_0 = 0, \quad V_{0tt} + W_0 = 0, \tag{11}$$

and it is easy to get the solution as

$$W_0(x,t) = A(x,\tau)e^{it} + c.c., \quad V_0(x,t) = B(x,\tau)e^{it} + c.c., \tag{12}$$

where *c.c.* represents corresponding complex conjugate and $\tau = \varepsilon|\lambda_M|t/2$ is a slow time variable. The solvability condition requires A and B satisfy the following coupled nonlinear differential equations

UNCORRECTED PROOF

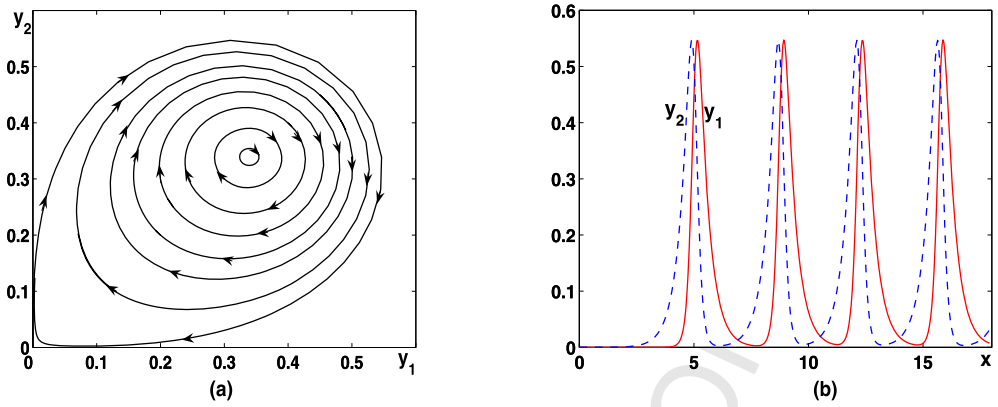

Fig. 4. (a) The phase portrait for the case $\gamma = 0$ with $\lambda_M = -0.21$, $\lambda_E = 0.45$, $\alpha = 1$, $\epsilon_l = 2$. (b) The numerical solution corresponds to the homoclinic orbit shown in Fig. 4(a).

$$i\frac{\partial A}{\partial \tau} + \frac{\partial B}{\partial x} = \frac{1}{\lambda_M}[(\lambda_M + \lambda_E)B - i\gamma A + \frac{\alpha}{\epsilon_l}|A|^2 A], \tag{13}$$

$$i\frac{\partial B}{\partial \tau} - \frac{\partial A}{\partial x} = \frac{1}{\lambda_M}[(\lambda_M + \lambda_E)B + i\gamma B + \frac{\alpha}{\epsilon_l}|B|^2 B]. \tag{14}$$

For the case of $\gamma = 0$, the exact solitary wave solutions of Eqs. (13) and (14) have been intensively studied in many systems. In the following we pay much attention on the stationary solutions of Eqs. (13) and (14) by making the transformation [12,13]

$$y_1 = |A|^2,\ y_2 = |B|^2,\ y_3 = AB^* + A^*B,\ y_4 = i(AB^* - A^*B). \tag{15}$$

Eqs. (13) and (14) can be rewritten as a real ordinary differential equation (ODE) system

$$\frac{dy_1}{dx} = \frac{1}{\lambda_M}[2(\lambda_M + \lambda_E)y_1 - \gamma y_4 + \frac{\alpha}{\epsilon_l}y_2 y_3], \tag{16}$$

$$\frac{dy_2}{dx} = \frac{1}{\lambda_M}[-2(\lambda_M + \lambda_E)y_2 + \gamma y_4 - \frac{\alpha}{\epsilon_l}y_1 y_3], \tag{17}$$

$$\frac{dy_3}{dx} = -\frac{2}{\lambda_M}\frac{\alpha}{\epsilon_l}(y_1^2 - y_2^2), \tag{18}$$

$$\frac{dy_4}{dx} = \frac{2\gamma}{\lambda_M}(y_1 - y_2). \tag{19}$$

If $\gamma = 0$ in Eqs. (16), (17), (19), there is an invariant

$$y_3 = -\frac{2\alpha}{\epsilon_l}\frac{1}{\lambda_M + \lambda_E}(y_1^2 + y_2^2), \tag{20}$$

and the real ODE system becomes a two-dimensional integrable system

$$\frac{dy_1}{dx} = \frac{1}{\lambda_M}[2(\lambda_M + \lambda_E)y_1 - \frac{2\alpha^2}{\epsilon_l^2(\lambda_M + \lambda_E)}y_2(y_1^2 + y_2^2)], \tag{21}$$

$$\frac{dy_2}{dx} = \frac{1}{\lambda_M}[-2(\lambda_M + \lambda_E)y_2 + \frac{2\alpha^2}{\epsilon_l^2(\lambda_M + \lambda_E)}y_1(y_1^2 + y_2^2)]. \tag{22}$$

It is helpful to use the method of qualitative analysis of dynamical systems and consider possible solutions of Eqs. (21) and (22) in the phase plane (y_1, y_2). Attention should be paid to separatrixes, which correspond to different kinds of soliton solutions. We can see there are two equilibrium points $(0, 0)$ and $(\epsilon_l|(\lambda_M + \lambda_E)/(\sqrt{2}\alpha)|, \epsilon_l|(\lambda_M + \lambda_E)/(\sqrt{2}\alpha)|)$ in Eqs. (21), (22). The Jacobian matrix of Eqs. (21) and (22) is

$$\begin{pmatrix} \frac{1}{\lambda_M}[2(\lambda_M + \lambda_E) - \frac{4\alpha^2}{\epsilon_l^2(\lambda_M + \lambda_E)}y_1 y_2] & \frac{1}{\lambda_M}[-\frac{2\alpha^2}{\epsilon_l^2(\lambda_M + \lambda_E)}(y_1^2 + 3y_2^2)] \\ \frac{1}{\lambda_M}[\frac{2\alpha^2}{\epsilon_l^2(\lambda_M + \lambda_E)}(3y_1^2 + y_2^2)] & \frac{1}{\lambda_M}[-2(\lambda_M + \lambda_E) + \frac{4\alpha^2}{\epsilon_l^2(\lambda_M + \lambda_E)}y_1 y_2] \end{pmatrix}. \tag{23}$$

For the equilibrium points $(0, 0)$, there are two different real eigenvalues $\pm 2(\lambda_M + \lambda_E)/\lambda_M$, then $(0, 0)$ is a saddle point. For another equilibrium points $(\epsilon_l|(\lambda_M + \lambda_E)/(\sqrt{2}\alpha)|, \epsilon_l|(\lambda_M + \lambda_E)/(\sqrt{2}\alpha)|)$, the eigenvalues are $\pm 4(\lambda_M + \lambda_E)/\lambda_M i$, so it is a center point. There is only one type of separatrix curves, i.e., homoclinic orbit. The phase portraits of the system and the numerical simulation corresponding to homoclinic orbit are exhibited in Fig. 4(a) and Fig. 4(b) respectively.

For our most interesting $\mathcal{PT}$-symmetry system with $\gamma \neq 0$, Eqs. (16)–(19) have an invariance

$$y_3 = -\frac{2\alpha}{\epsilon_l}\frac{1}{\lambda_M + \lambda_E}(y_1^2 + y_2^2 + \frac{1}{2}y_4^2). \tag{24}$$

UNCORRECTED PROOF

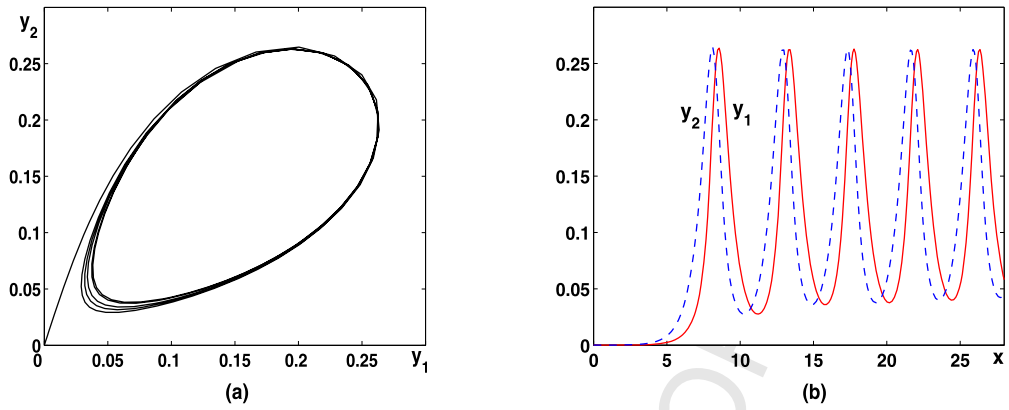

Fig. 5. (a) The phase portrait for the case $\gamma = 0.1$ with $\lambda_M = -0.21$, $\lambda_E = 0.45$, $\alpha = 1$, $\epsilon_l = 2$. (b) The numerical solution corresponds to the homoclinic orbit shown in Fig. 5(a).

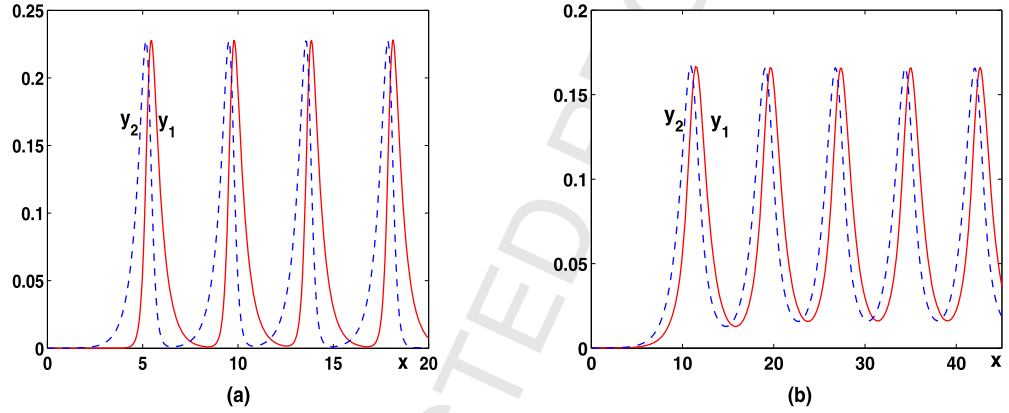

Fig. 6. (a) The numerical solution for the case $\gamma = 0$ with $\lambda_M = -0.1$, $\lambda_E = 0.2$, $\alpha = 1$, $\epsilon_l = 2$. (b) The numerical solution for the case $\gamma = 0.09$ with $\lambda_M = -0.1$, $\lambda_E = 0.2$, $\alpha = 1$, $\epsilon_l = 2$.

The real ODE system (16)–(19) can be reduced into the three-dimensional system,

$$\frac{dy_1}{dx} = \frac{1}{\lambda_M}[2(\lambda_M+\lambda_E)y_1 - \frac{2\alpha^2}{\epsilon_l^2(\lambda_M+\lambda_E)}y_2(y_1^2+y_2^2+\frac{1}{2}y_4^2) - \gamma y_4], \tag{25}$$

$$\frac{dy_2}{dx} = \frac{1}{\lambda_M}[-2(\lambda_M+\lambda_E)y_2 + \frac{2\alpha^2}{\epsilon_l^2(\lambda_M+\lambda_E)}y_1(y_1^2+y_2^2+\frac{1}{2}y_4^2) + \gamma y_4], \tag{26}$$

$$\frac{dy_4}{dx} = \frac{2\gamma}{\lambda_M}(y_1 - y_2), \tag{27}$$

with the corresponding Jacobian matrix

$$\begin{pmatrix} \frac{1}{\lambda_M}[2(\lambda_M+\lambda_E) - \frac{4\alpha^2}{\epsilon_l^2(\lambda_M+\lambda_E)}y_1y_2] & \frac{1}{\lambda_M}[-\frac{2\alpha^2}{\epsilon_l^2(\lambda_M+\lambda_E)}(y_1^2+3y_2^2)+\frac{1}{2}y_4^2] & \frac{1}{\lambda_M}[-\frac{2\alpha^2}{\epsilon_l^2(\lambda_M+\lambda_E)}y_2y_4-\gamma] \\ \frac{1}{\lambda_M}[\frac{2\alpha^2}{\epsilon_l^2(\lambda_M+\lambda_E)}(3y_1^2+y_2^2+\frac{1}{2}y_4^2)] & \frac{1}{\lambda_M}[-2(\lambda_M+\lambda_E) + \frac{4\alpha^2}{\epsilon_l^2(\lambda_M+\lambda_E)}y_1y_2] & \frac{1}{\lambda_M}[\frac{2\alpha^2}{\epsilon_l^2(\lambda_M+\lambda_E)}y_1y_4+\gamma] \\ \frac{2\gamma}{\lambda_M} & -\frac{2\gamma}{\lambda_M} & 0 \end{pmatrix}. \tag{28}$$

One finds the Jacobian matrix (28) at the equilibrium point $(0,0,0)$ has three eigenvalues: 0 and $\pm 2\sqrt{(\lambda_M+\lambda_E)^2-\gamma^2}/|\lambda_M|$. Then the equilibrium point is a saddle when $0 < \gamma < |\lambda_M+\lambda_E|$, while it is a center when $\gamma > |\lambda_M+\lambda_E|$, which means there is a bifurcation from saddle to center at $\gamma = |\lambda_M+\lambda_E|$. If the condition $0 < \gamma < |\lambda_M+\lambda_E|$ is satisfied, the equilibrium point is a saddle point, and the separatrix curve is homoclinic orbit as shown in Fig. 5(a). The soliton-like localized modes correspond to separatrix curves are presented in Fig. 5(b) numerically. If the electric and magnetic coupling coefficients are smaller, i.e., $\lambda_M = -0.1$, $\lambda_E = 0.2$, we can obtain the solutions numerically shown in Fig. 6. Soliton-like localized modes also exist within the allowable parameter range, but the amplitude is reduced and the width is increased.

For the experimental 1D SRRs array system, the analytical expressions for the resonant frequency of single ring SRR is $\omega_s = 1/\sqrt{LC}$ with the kinetic inductance $L = (2\pi r - g)/(S\omega_p^2\varepsilon_0)$. The total capacitance C is the sum of the surface capacitances $C_{surf} = 2\varepsilon_0(h+w)/\pi\log(4r/g)$ and the gap capacitances $C_{gap} = \varepsilon_0 hw/g + \varepsilon_0(h+g+w)$, where ω_p is the plasma frequency, S is the area of the ring's cross section. If the parameters are taken as $w = 0.1r$, $h = r$, $g = 0.1r$, $r = 0.3\mu m$ for the SRR width, height, gap width, mean radius, respectively, the resonant frequency SRR is about 57.7 THz [27]. Both magnetic and electric coupling parameter can be adjusted by the distance of the neighboring elements. The analytic expression of mutual inductance is given as $M = \mu_0(\pi r^2)^2/(\pi a^2)$ for the planar

UNCORRECTED PROOF

geometry which the gaps have the same direction [23]. We can calculate the magnetic coupling $\lambda_M = 2M/L = 0.28$ if the distance of the neighboring elements is chosen $a/2 = 2.7r$, then the magnetic coupling coefficient is expected less than 0.28 in the far configuration in our model. The experimental and numerical results in Fig. 3 in Ref. [21] show that the magnetic coupling λ_M can be achieved from 0.1 to 0.21 and electric coupling λ_E from 0.1 to 0.45 with decreasing the distance of the neighboring elements. Scaling down the size of SRRs to THz does not change the character of the coupling mechanisms in either of the considered orientations numerically shown in Fig. 4 in Ref. [21]. The linear permittivity can be taken as $\epsilon_l = 2$ [23]. Although $\mathcal{PT}$-symmetry has been realized in many systems, experimental investigation of nonlinear localized modes in $\mathcal{PT}$-symmetric system is currently underway.

4. Conclusions

In conclusion, we have investigated a chain of SRR dimers which all the SRRs are equidistant but with opposite orientations of the gaps. The $\mathcal{PT}$-symmetry condition is satisfied either by introducing gain and loss or by alternating electric and magnetic coupling. Much attention has been paid to parameter space where a $\mathcal{PT}$-symmetric phase is stable, i.e., all eigenvalues are real, and where $\mathcal{PT}$-symmetry breaking occurs, i.e., the eigenvalues acquire imaginary part. It can be seen the loss are as important as the gain. In the presence of Kerr nonlinearity, we demonstrate such $\mathcal{PT}$-symmetric dimers chain supports soliton structures. These localized structures is studied in the phase plane and their numerical results are proposed. Despite the presence of gain and loss, the soliton solutions behave in way similar to that of conservative solitons in standard Hermitian nonlinear lattices. The above controllable nonlinear dynamical behavior result from gain, loss and nonlinearity which may have some extended application in nonlinear dissipative systems. We hope our results will provide an alternative way of generating localized modes, and stimulate much interest in nonlinear $\mathcal{PT}$-symmetric metamaterials.

Acknowledgements

This work was financially supported by the National Natural Science Foundation of China (Grant No. 41675133) and the Natural Science Foundation of Jiangsu Province (Grant No. BK20141480 and Grant No. BE2015003-4).

References

[1] A. Guo, G.J. Salamo, D. Duchesne, R. Morandotti, M. Volatierravat, V. Aimez, G.A. Siviloglou, D.N. Christodoulides, Phys. Rev. Lett. 103 (2009) 093902.
[2] J. Schindler, A. Li, M.C. Zheng, F.M. Ellis, T. Kottos, Phys. Rev. A 84 (2011), 040101(R).
[3] A. Regensburger, C. Bersch, M.A. Miri, G. Onishchukov, D.N. Christodoulides, U. Peschel, Nature 488 (2012) 167.
[4] L. Feng, Y. Long Xu, W.S. Fegadolli, M.H. Lu, J.E.B. Oliveira, V.R. Almeida, Y.F. Chen, A. Scherer, Nat. Mater. 12 (2013) 108.
[5] C.M. Bender, S. Boettcher, Phys. Rev. Lett. 80 (1998) 5243.
[6] C.M. Bender, S. Boettcher, P.N. Meisinger, J. Math. Phys. 40 (1999) 2201.
[7] C.E. Ruter, K.G. Makris, R.E. Ganainy, D.N. Christodoulides, M. Segev, D. Kip, Nat. Phys. 6 (2010) 192.
[8] Y.L. Xu, W.S. Fegadolli, L. Gan, M.H. Lu, X.P. Liu, Z.Y. Li, A. Scherer, Y.F. Chen, Nat. Commun. 7 (2016) 11319.
[9] S.V. Suchkov, A.A. Sukhorukov, J. Huang, S.V. Dmitriev, C. Lee, Y.S. Kivsha, Laser Photonics Rev. 10 (2016) 177.
[10] S.V. Dmitriev, A.A. Sukhorukov, Y.S. Kivshar, Opt. Lett. 35 (2010) 2976.
[11] C. Hang, Y.V. Kartashov, G.X. Huang, V.V. Konotop, Opt. Lett. 40 (2015) 2758.
[12] P.G. Kevrekidis, D.E. Pelinovsky, D.Y. Tyugin, J. Phys. A, Math. Theor. 46 (2013) 365201.
[13] D.H. Wang, A.B. Aceves, Phys. Rev. A 88 (2013) 043831.
[14] D.R. Smith, J.B. Pendry, M.C.K. Wiltshire, Science 305 (2004) 788.
[15] F. Hesmer, E. Tatartschuk, O. Zhuromskyy, A.A. Radkovskaya, M. Shamonin, T. Hao, C.J. Stevens, G. Faulkner, D.J. Edwards, E. Shamonina, Phys. Status Solidi B 244 (2007) 1170.
[16] O. Sydoruk, A. Radkovskaya, O. Zhuromskyy, E. Shamonina, M. Shamonin, Phys. Rev. B 73 (2006) 224406.
[17] D.A. Powell, M. Lapine, M.V. Gorkunov, I.V. Shadrivov, Y.S. Kivshar, Phys. Rev. B 82 (2010) 155128.
[18] D.R. Chowdhury, R. Singh, M. Reiten, J. Zhou, A.J. Taylor, J.F. O'Hara, Opt. Express 19 (2011) 10679.
[19] E. Shamonina, V.A. Kalinin, K.H. Ringhofer, L. Solymar, Electron. Lett. 38 (2002) 371.
[20] E. Shamonina, V.A. Kalinin, K.H. Ringhofer, L. Solymar, J. Appl. Phys. 92 (2002) 6252.
[21] A. Radkovskaya, O. Sydoruk, E. Tatartschuk, N. Gneiding, C.J. Stevens, D.J. Edwards, E. Shamonina, Phys. Rev. B 84 (2011) 125121.
[22] H. Liu, S.N. Zhu, Laser Photonics Rev. 7 (2013) 882.
[23] A.A. Zharov, I.V. Shadrivov, Y.S. Kivshar, Phys. Rev. Lett. 91 (2003) 037401.
[24] W.N. Cui, Y.Y. Zhu, H.X. Li, S.M. Liu, Phys. Rev. E 81 (2010) 016604.
[25] W.N. Cui, H.X. Li, M. Sun, L.B. Bu, Phys. Lett. A 381 (2017) 1950.
[26] N. Lazarides, G.P. Tsironis, Phys. Rev. Lett. 110 (2013) 053901.
[27] V. Delgado, O. Sydoruk, E. Tatartschuk, R. Marques, M.J. Freire, L. Jelinek, Metamaterials 3 (2009) 57.

UNCORRECTED PROOF